

Study of the Effects of Solution Types on Concentration of Iron Oxide by Pulsed Laser Ablation in Liquid

¹Rusul Al-Obaidy, ¹Adawiya J. Haider, ²Sharafaldin Al-Musawi*, ³Norhana Arsad

¹Department of Applied Sciences, University of Technology – Iraq

²College of Food Sciences, Al-Qasim Green University – Iraq

³UKM—Department of Electrical, Electronic and Systems Engineering, Faculty of Engineering and Built Environment, Universiti Kebangsaan Malaysia

ARTICLE INFO

Article history:

Received: May, 01, 2022

Accepted: July, 07, 2022

Available online: March, 10, 2023

Keywords:

SPION,
Eco-friendly,
Drug delivery

*Corresponding Author:

Sharafaldin Al-Musawi
dr.sharaf@biotech.uoqasim.edu.iq

ABSTRACT

In this work, the development of nanosystems by Pulsed Laser Ablation in Liquid (PLAIL) is of considerable importance to expand their biomedical applications, such as drug delivery. In the present study, we focus on the conditions of the preparation Nd: YAG laser wavelength 266 nm and two different laser fluency (10,28) J/cm² to control the concentration and size stability of superparamagnetic iron oxide nanoparticles (SPION) prepared by PLAIL. The characteristics of SPION are investigated by energy-dispersive X-ray spectroscopy (EDX) spectra which showed strong peaks of Fe and O. Magnetic characteristics of iron oxide nanoparticles indicated superparamagnetic properties of SPION and suitable physical stability. Optical and chemical properties of SPION were investigated using UV-visible spectra (UV) and infrared Fourier transformed spectroscopy (FTIR). Scanning electron microscopy (SEM) was used to obtain surface morphological studies of SPION. Results showed that SPION is the only cubic shape, the peak absorption shifted toward short wavelengths with optimum concentration to the SPION in double deionized water (DDW) and in Acetone (0.75,0.33) mg/ml respectively, at high laser fluence 28 J/cm², and this enhancement of value is due to particle size and color resultant in a solution. Eventually, this product has the optimal SPION specialty ratio of SPION in the DDW solution at 53.89%, and the size is very suitable for drug delivery applications.

<https://doi.org/10.53293/jasn.2022.5025.1172>, Department of Applied Sciences, University of Technology - Iraq.
© 2023 The Author(s). This is an open access article under the CC BY license (<http://creativecommons.org/licenses/by/4.0/>).

1. Introduction

The word "Nano" is derived from the Greek language, which includes particles in the size range of 1 to 100 nm. Nanoparticles have novel physicochemical characteristics compared to other solid bulk objects, that is, they have large reactive areas and exceptional electronic properties [1-4]. New morphologies have been created employing a variety of synthetic methods [5, 6]. The main goal is to build NP that is ecologically friendly and can be used to address future environmental problems [7-9]. Metal nanoparticles are commonly prepared by evaporation–

condensation, which could be carried out using a tube furnace at atmospheric pressure [13]. Other preparation methods are lithography [14], ball milling [15], arc discharge, and pulsed laser ablation [16]. All these methods require serious handling and safety must be taken into account when working with NPs [14-16]. Laser ablation and nanoparticle generation in liquids is a unique and efficient technique to generate [20], excite, fragment, and conjugate a wide variety of nanostructures in a scalable and clean way [21]. Pulsed laser ablation in liquids is one of the modern technologies that can create very dense nanostructures in a variety of shapes depending on the type of liquid used and can be clad with other materials for medical and biological uses, such as core-shell design, with high purity and accuracy, to obtain a closure that can be used in the drug delivery technique [22]. There are many area applications of Fe_3O_4 nanoparticles, such as Li-ion batteries [23], biomedical [24, 25], etc. summarized in Fig. 1.

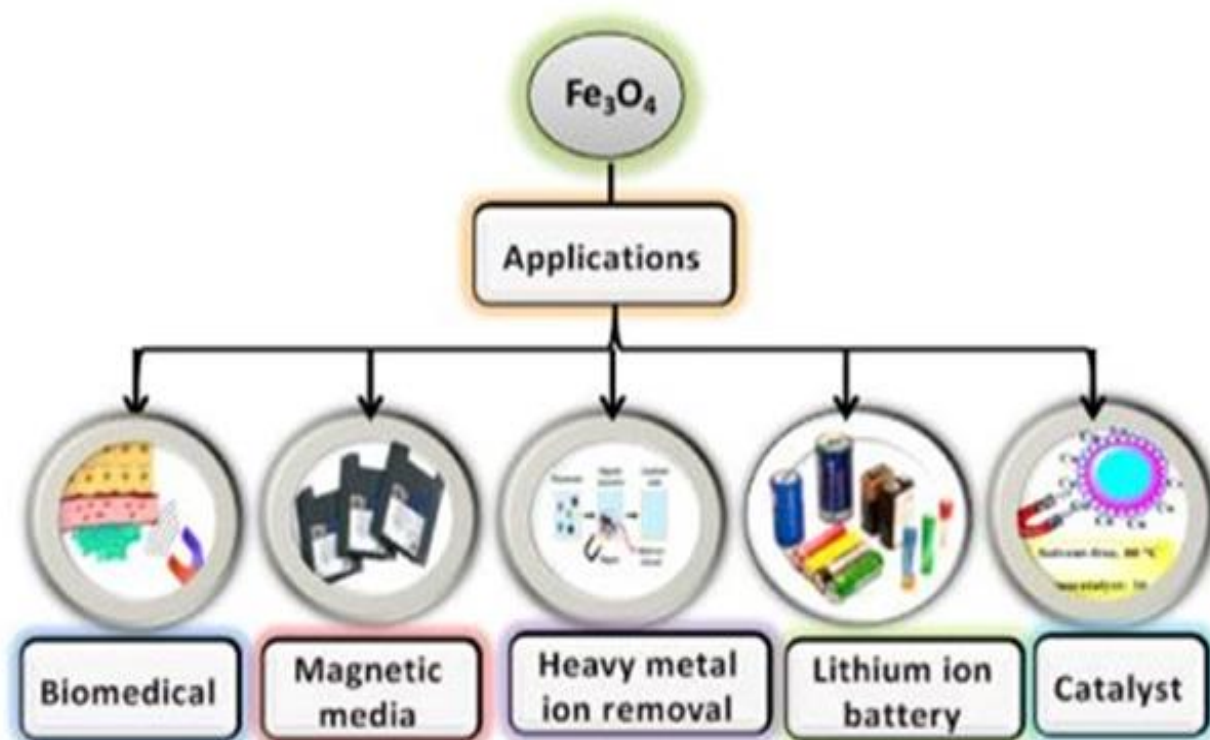


Figure 1: The Schematic presentation of the Fe_3O_4 applications.

Magnetite is generated from a cubic packing of oxygen with cations at the interstitial tetrahedral and octahedral sites, where Fe (II) and Fe (III) cations are disordered at the octahedral sites, whereas the Fe (III) cation entirely occupies the tetrahedrons. The material is ferrimagnetic up to Curie temperature (858 K) [25]. When exposed to air, Fe_3O_4 crystallites commonly develop Fe_2O_3 layers on their surfaces. However, magnetite nanoparticles with diameters of less than 30 nm are superparamagnetic [26], meaning that they do not have magnetization and are less prone to aggregation. They also outperform metallic nanoparticles in terms of chemical stability and biocompatibility [27]. Among the most common methods for making these particles are green hydrothermal synthesis, coprecipitation, and laser ablation [28]. The scientific community is interested in laser ablation as a synthesis method. For example, Yang mentions in his review article that liquid laser ablation is a chemically simple and clean synthesis that does not require severe temperatures or pressures [29]. These benefits enable the use of solid and liquid phases to create composite nanostructures [30, 31]. This study investigated the control of the liquid types and laser fluency on the concentration and stoichiometry of the iron oxide NPs fabricated by nanosecond and third-harmonic generation (THG) laser ablation. For a generation, different types of liquids such as water, acetone ethanol, and methanol were used. The elements' concentrations were measured using EDS spectra for a pure Fe plate, and then UV-vis spectroscopy of all NPs prepared in different liquids was used to investigate

absorbance, SPION concentration, and stability with statistical analyzes. Lastly, we used FTIR spectra for the chemical compositions of SPION, after obtaining a homogeneous SPION colloid with high laser fluence.

2. Experimental Procedures

2.1. Preparation of SPION

Fig. 2 shows the practical arrangement for preparing a SIPON colloid by removal of pulsed laser technology in a liquid using a pulsed Nd: A YAG laser (type HUAFEI), with a wavelength of 226 working with the third harmonic generation technique (THG). A high purity iron plate (Fe) (Sigma Aldrich (St.Louis MO, USA), 99.5 %, geometry(10×10×0.5) cm was used to prepare SIPONs. The elemental analysis of the target materials was measured by an EDX device. This plate was cleaned with an ultrasonic cleaner, then washed with ethanol, acetone, and deionized water to remove any remaining organic compounds after cutting them into small pieces with dimensions of 1x1 cm. Table 1 illuminates the material points and laser parameters that were utilized in the experimental part.

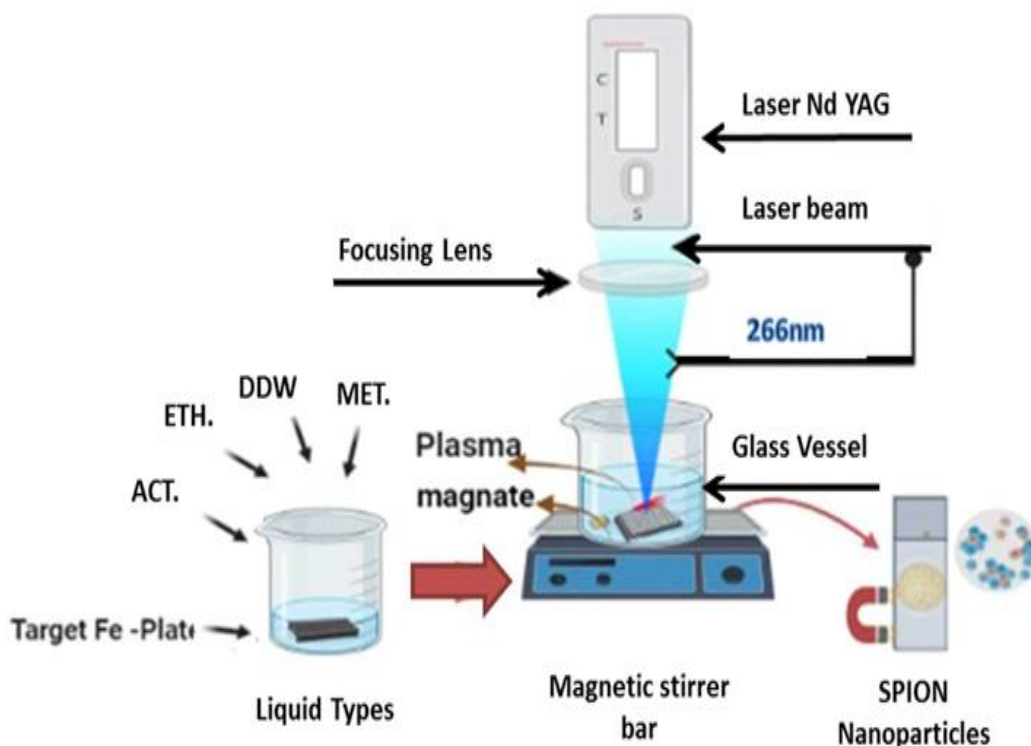


Figure 2: Aschematic presentation of the experimental setup for SPION prepared by PLAIL with different types of liquid.

Table 1: Laser parameters and materials used in the experimental setup for prepared SPION.

Parameters		Details
Laser beam	Wavelength	266 nm
	Pulse repetition rate	1 Hz
	Duration Spot Size	9 ns
	Spot Size	(1.5-2)mm
	Fluence	(10,28) J/cm ²
Materials	Target	Fe Plate
	liquid	Double-ionized water, acetone, methanol, ethanol

The target was then placed inside a glass beaker containing a small volume of 10 mL of liquid 2 millimeters above the target. This liquid consists of DDW, acetone, methanol, and ethanol, which are used in this process. All laser parameters used are illustrated in Table 1. The beam diameter is 2 mm was used for laser ablation. Focusing the laser beam on the target inside the beaker glass placed on a magnetic stirrer at 700 rpm rounds.

The laser fluences used are 10, and 28 J/cm² with shots of 100 pulses which can be controlled by the digital screen for 20 minutes at room temperature. Stopped the ablation process every three minutes [12-14, 30, 31]. The laser pulse strikes the target from above impinging perpendicularly onto the target. These experimental procedures were chosen to obtain valid colloidal stability [34], following the indications of our previous experiments. The maximum absorbance of the nanoparticle solution was determined by using a UV-visible

2.2 Characterization of SPION NPs

Characterization was carried out using various approaches, such as optical properties study by absorbance (UV-VISB). The optical properties of SPION NPs were measured using a double beam UV-visible spectrophotometer (Aquarius 7000) in the range of (200-800) nm and the morphology of SPIONs was studied by (SEM). The chemical properties study by FTIR spectral: Changes in the composition of various nanoparticles were recorded on a Nicolet 6700 infrared detector (Thermo Fisher Scientific, USA). SPION NPs were pressed with KBr to obtain the pellets using a pressure of 300 kg/cm². The FTIR spectra of the prepared samples were acquired by averaging 32 interferograms in the range of 1000-4000 cm⁻¹ with a resolution of 2 cm⁻¹.

3. Results and Discussion

3.1 EDX analysis for the Fe plate

Fig. 3 shows an EDX spectrum of Fe target and the associated analyses in Table 2. The K series X-ray distinguishes all elements. Elements' concentrations were measured using EDX. We used elemental analysis to evaluate the chemical composition of a material. Rather than structural consistency, variations were attributed to the short duration of testing and background and contaminant interferences [35]. The A-elements' energies may interfere with the backdrop or SEM chamber's energies, causing the background in this figure.

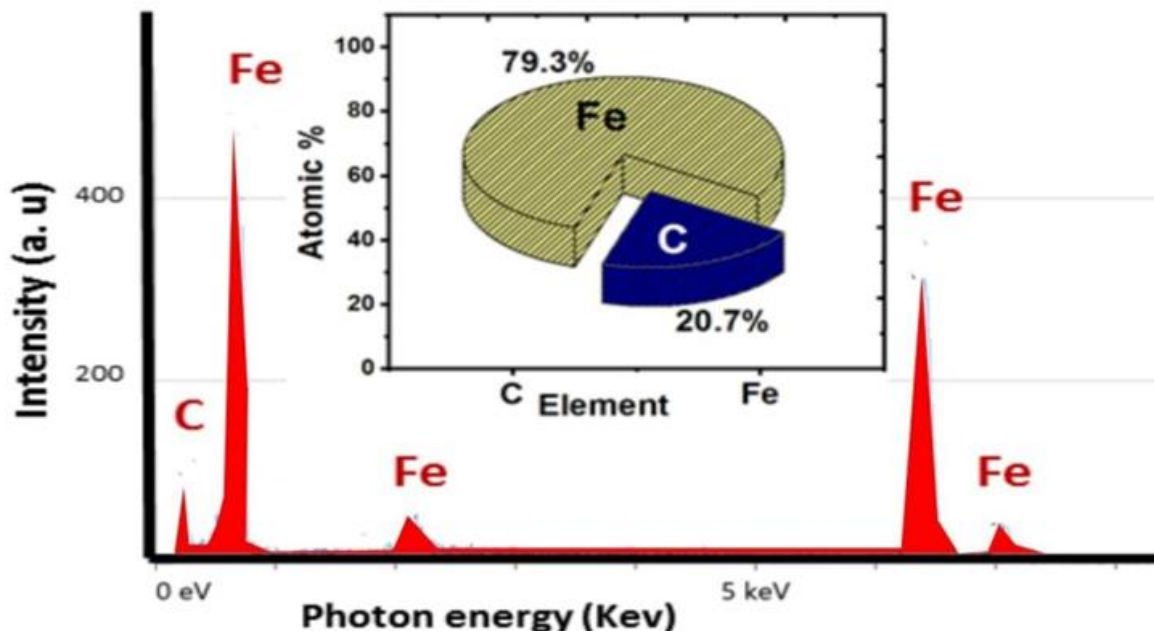


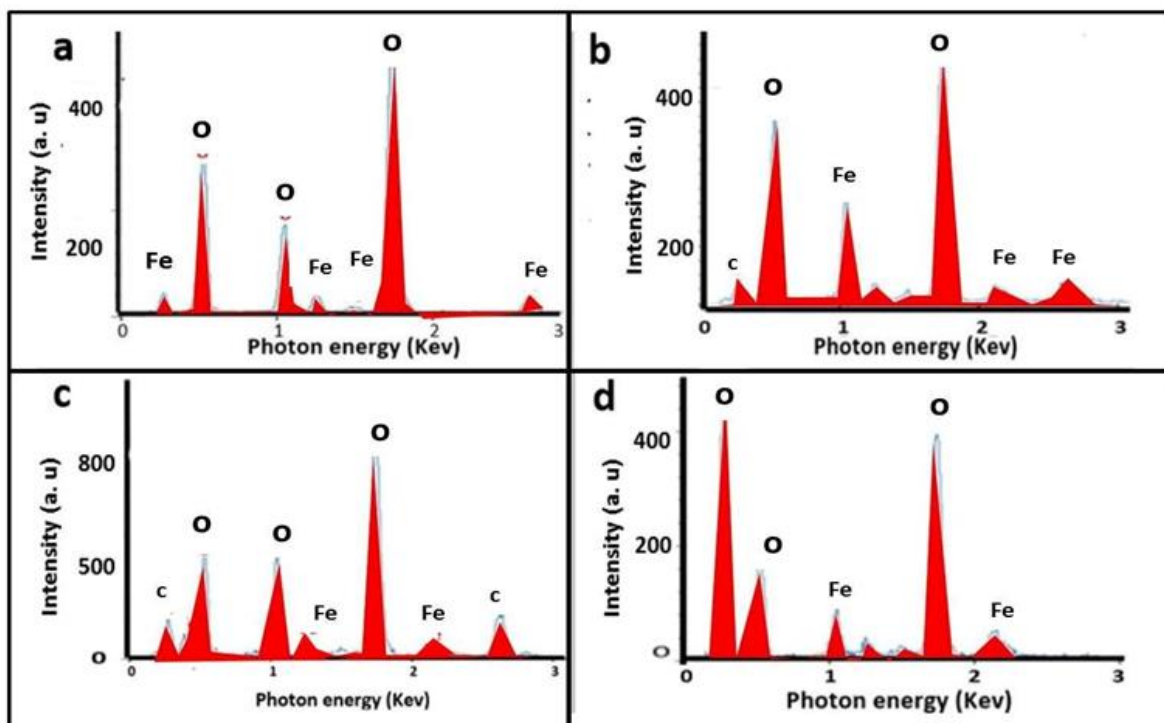
Figure 3: EDX spectrum of Fe plate before ablation by LPAIL.

Table 2: Summarized the elements' weight and atomical percentage of Fe plate by EDX before ablation process by laser in liquid.

Element	Weight %	Atomic % Error	Atomic %	Weight % Error
Iron (Fe)	94.7	1.9	79.3	2.2
Carbon (C)	5.3	1.2	20.7	0.3

3.2 EDX Analysis for the Prepared SPION NPs in Different Liquids after Ablation Process

Fig. 4 shows an EDX spectra of colloidal SPION prepared in different liquids (DDW, ethanol, methanol, and acetone) after ablation of the Fe target. The EDX spectra showed strong peaks of Fe and O. The components of Fe_3O_4 were formed by the Nd laser: YAG with operating wavelength of 226 nm working with THG and the associated analyses summarized in Table 3. Fig. 3 did not show any oxygen peak in the EDX spectrum, because it presents different liquids before the ablation process. Fig. 4 indicates the high intensity of the oxygen element after the ablation of the Fe plate in all different liquids. The weight percentages values of iron and oxygen elements for each liquid were listed in Table 3, without weight percentages values of carbon due to their very low intensity. The morphology of Fe_3O_4 NPs was examined by the scanning electron microscope-Energy Dispersive X-Ray Spectrometry (SEM-EDX). The results shown in Fig. 4 is only for SPION in ethanol, and other liquids SEM results have observed by other researchers. Fig. 5 a show the SEM image of small cubic nanoparticles of SPIONs with a single shape, such as quasi-cubical and without dense nanoparticles or aggregation, and Fig. 5b displays a histogram of the distribution of granularity for SPIONs of similar size at a scale of less than 50 nm with high frequency%. Therefore, this means a low NPs concentration in this sample. In addition, these results are agreement with EDX results shown in Fig. 4b and elemental weight of 2.2 % iron and 85.6% of particles produced by laser ablation in pure ethanol with wavelength 266 nm observed in Table 3. Also, of the same condition with similarly, Lian *et. al.*, (2009) [35].

**Figure 4:** EDX spectra for iron oxide prepared by laser in different liquids, a-DDW, b-ethanol, c-Methanol, and d-acetone.

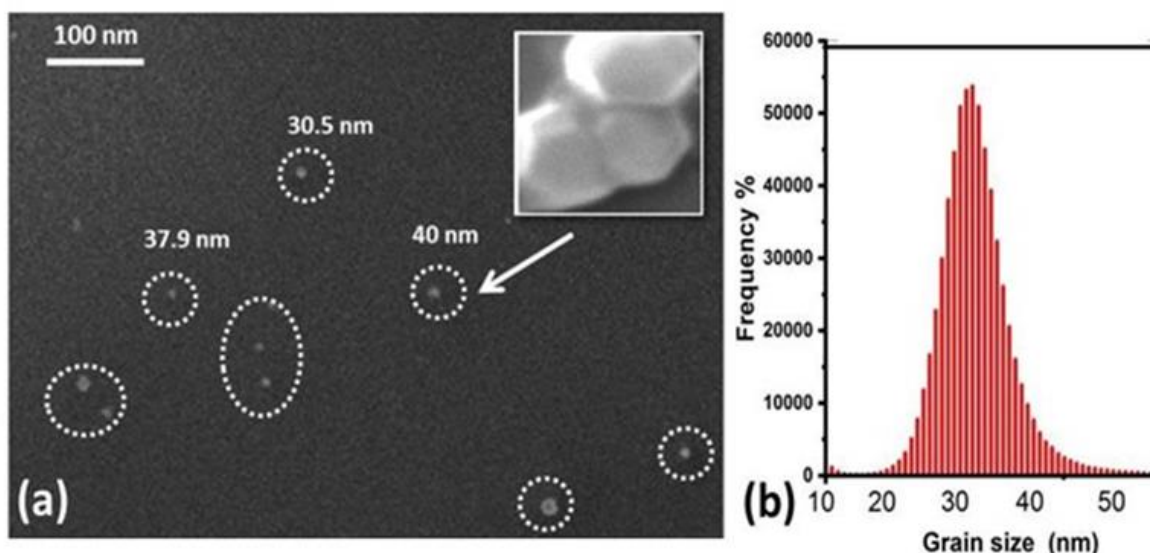


Figure 5: The morphological characterization of the SPIONs prepared in liquid by laser with a wavelength of 266 nm and 10 J/cm² laser fluence for 100 pulses (a) SEM micrographs showing the morphologies of cubic SPIONs in ethanol, and (b) a histogram of the grain size distribution of the SPIONs.

Table 3: Summarize elements' weight percentage and atomic ratios of the SPION NPs obtained from EDX results after ablation of Fe plate in liquids by laser.

Element	Liquid	Weight %	Atomic%	Weight % Error	Atomic% Error
(Iron)Fe	DDW	3.5	1.0	1.3	0.4
(Oxygen)O	DDW	96.5	99.0	0.9	0.9
(Iron)Fe	Ethanol	2.2	0.6	1.2	1.2
(Oxygen)O	Ethanol	85.6	83.5	1.2	1.2
(Iron)Fe	Methanol	9.2	2.6	1.9	0.5
(Oxygen)O	Methanol	69.8	69.5	2.1	2.1
(Iron)Fe	Acetone	1.9	0.5	1	0.2
(Oxygen)O	Acetone	51.4	45.0	1.6	1.4

3.3 UV-visible Spectroscopy Analysis for Study of the effect of Solution Types and Laser Fluence on the Concentration of SPIONs NPs.

Fig. 6 a,b,c, and d explains the absorbance spectra of prepared SPION in DDW, ethanol, methanol, and acetone by laser with a wavelength of 266 nm at laser fluences of 10 and 28 J/cm². This article describes the effect of pulse energy wavelength penetrating in a liquid with minimum spot size on the surface of the ablation target for all solutions. Laser ablation in these liquid types can be used to create NPs with a variety of laser fluences.

Table 4 with Fig. 6 shows absorbance values of the SPIONs NPs prepared in low fluence density at 10 J/cm² (black line) and at a higher fluence 28 J/cm² (red line) with a wavelength of 266 nm, at both peaks, absorbance broadband in (a) DDW and in (b) ethanol, highest absorbance is 0.079, 0.765 at 222, 243nm and 0.082, 0.923 at 309, 289nm, respectively. A change in absorbance with a width band shift in the optical absorption towards a longer wavelength region of about (200-300) nm was observed due to the generation of large NPs [36, 37]. While at both peaks absorbance in (c) methanol and (d) acetone liquids had the highest absorbance 0.122, 0.177 at 322,325nm and 0.177,0.937 at 322,325nm, respectively, no change absorbance peaks and fixed at 300 nm wavelength region due to small size SPIONs and high stability in these liquids [13, 38, 39].

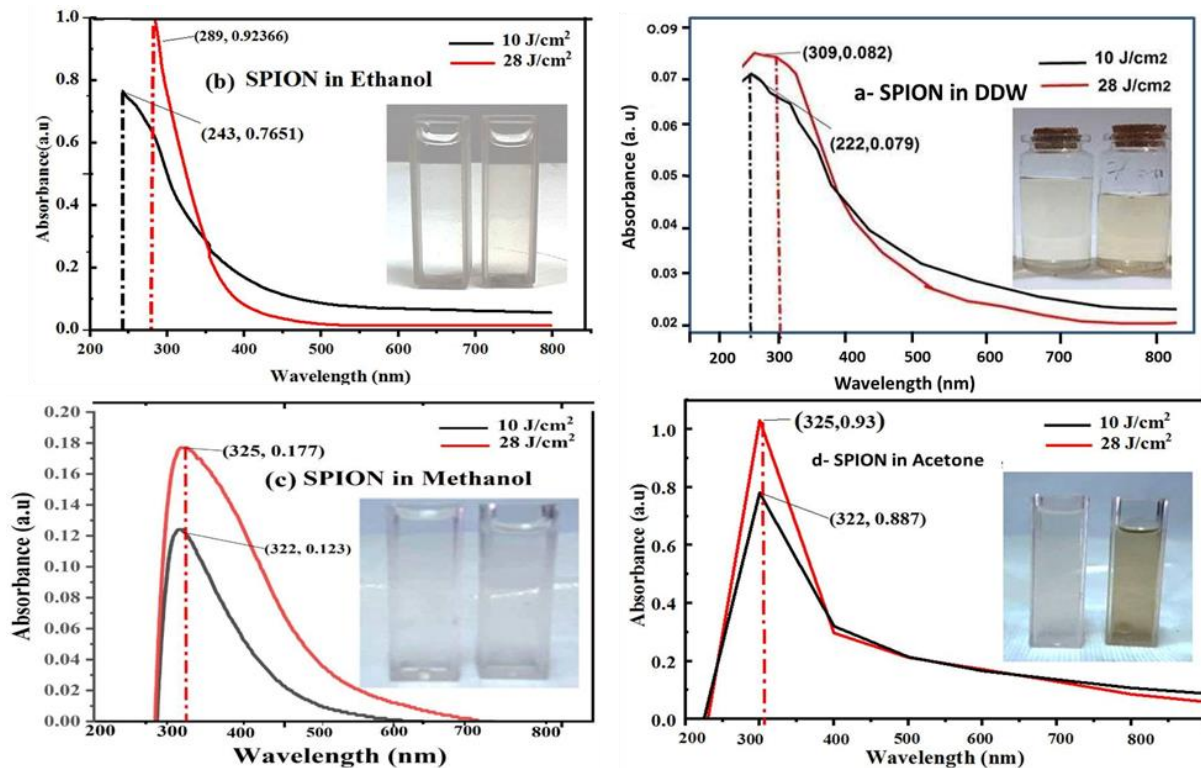


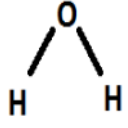
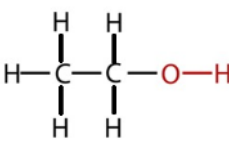
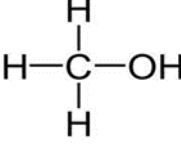
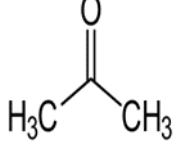
Figure 6: Absorbance spectra of SPION NPs prepared in different liquids with various fluences of 10 and 28 J/cm² with a wavelength of 266nm. Insertion images show the coloration of the suspensions with variety of laser fluences (a- DDW,b- ethanol, c, methanol, and d- Acetone).

Table 4: Optimal values of absorbance for SPIONs NPs with different laser fluences at wavelength 266 nm.

Laser Fluence (J/cm ²)	SPION Abs. DDW	SPION Abs. Ethanol	SPION Abs. Methanol	SPION Abs. Acetone
10	0.079	0.765	0.122	0.887
28	0.082	0.923	0.177	0.937

Also, it is seen a higher absorbance in all liquids in Fig. 6(b,c, and d), because of the effect of ethanol, methanol, and acetone, this shift could be due to the fragmentation resulting from high laser fluence and could be correlated with the presence of Fe⁺³ with carbon or with the plasmon resonance of the nanoparticles or it may be due to the Brillouin transitions of iron oxide and O⁻² F⁺² charge transfer for particles slightly smaller than ours. The efficiency of formation is dependent on the reactivity of the liquid with Fe atoms in the plasma plume, these observations are in good agreement with the experimental spectra results reported by Sastry *et al.* [40]. An increased in the concentration of NPs in acetone due to an increased laser influence does not make any substantial change in the characteristics of the component peaks except for a minor change in their relative intensities [10, 41]. Therefore, Fig. 6d shows that increasing laser fluence gives the highest optical absorption at 325 nm, due to the stability NPs in all laser fluences and is based on the insignificant effect of acetone; this shift could be due to large size nanoparticles [38, 42]. Also shown the broadening of the Plasmon peak in methanol and acetone are sharper than in water and ethanol because, in acetone and methanol, there is high energy of both linear and nonlinear absorption mechanisms, accompanied by fragmentation of existing nanoparticles. Additional irradiation of laser pulses onto colloidal solution via liquid-phase laser ablation can also be used to decrease the size of NPs, resulting in smaller fragments of NPs and high concentrations with a wavelength of 266 nm [43]. Therefore, acetone has good stabilizing power and serves as a superior liquid medium that keeps fine SPIONs free from ablation and oxidation. This phenomenon was discussed as a pioneer study by Barella, 2010 [44], and Table 5 summarize the formula and type formation of SPION in the different types of liquids [7, 44, 46].

Table 5: The chemical formulas of liquid types and SPION forms in the different liquids.

Liquid types	Water	Ethanol	Methanol	Acetone
Formula of liquid				
SPION forms after ablation in liquid	Fe ₃ O ₄ , Fe ₂ O ₃ Fe(OOH) ₂	Fe ₃ O ₄ , FeC ₃	Fe ₃ O ₄ , Carbon	Fe ₃ O ₄ , Carbon

In summary, stable and pure SPIONs have been synthesized by laser ablation in acetone without the presence of any surfactant and high dispersibility and single-phase purity, and as a result, changing the nature of the liquid environment is an easy way to have SPIONs with a different size distribution, high concentration, and high stability [47, 48]. Fig. 7 a and b shows the effect of laser fluences on the metal target depth in all liquids with an ablation rate, and constant wavelength of 266 nm. It is affected by the fluence laser utilized to create the iron oxide colloidal nanoparticles and an increase in the ablation rate with increasing laser fluence as shown in Fig. 7a. The color change of the suspension confirms the presence of Fe₃O₄ NP after ablation as shown in Fig. 7b.

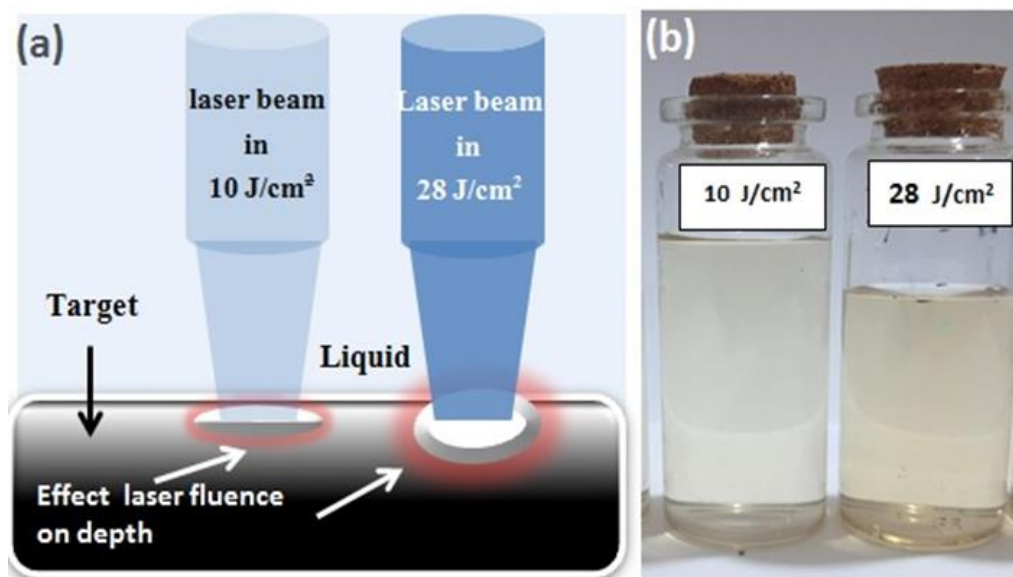


Figure 7: The laser ablation of Fe plate in liquid at (a) difference laser fluence, and (b) coloration of the suspensions prepared with different fluences (10 & 28) J /cm² with a fixed wavelength 226nm.

A sensitive balance with (0.0000) 4 digits was used to calculate the amount of ablated material from the target (plate) by laser ablation of materials. It is used to determine the mass concentration of nanoparticles. For this purpose, the target was weighed before and after the laser irradiation for each preparation condition. After drying the targets, the amount of ablated target mass ΔM and the iron oxide decoration ratio were calculated from the SPION concentration [49, 50]. Therefore, through this process, you will find from the results the highest concentration of SPION NP, especially in these types of liquid DDW and acetone, then methanol and ethanol which its value is 0.75,0.33, 0.25, and 0.21 mg/mL, respectively [51], at laser fluence 28 J/cm² and is 0.32,0.23,0.12 and 0.12 mg/mL at laser fluence 10 J/cm². Optimal values of SPIONs concentrations in different types of liquids are listed in Table 6.

Table 6: Optimum values of SPIONs concentrations in different types of liquids with wavelength 266 nm.

Liquid&Fluence J/cm ²	DDW 10	DDW 28	Ethanol 10	Ethanol 28	Acetone 10	Acetone 28	Methanol 10	Methanol 28
Weight mg /mL	0.32	0.75	0.12	0.21	0.23	0.33	0.12	0.25
Ratio of SPION %	36.10	53.89	19.12	29.28	23.31	30.99	19.12	29.89

The statistical analyzes in the Origin 2018 program and Table 6, concluded in Fig. 8 were obtained which shows the relationship between the maximum concentration of SPIONs at fluences of 10 and 28 J/cm² in different liquid types after laser ablation at wavelength 266 nm. Fig. 8 (a) at 10 J/cm² and (b) at 28 J/cm² agree with the other results studies in this work and shows a general decrease in absorbance and concentration SPION (red bar) of all liquids (DDW, ethanol, acetone, and methanol) at 0.32, 0.12, 0.23 and 0.12, while the SPION ratio (green bar) at 36.1%, 19.12%, 23.31%, and 19.12%, respectively in Fig. 8a with a decrease laser fluence in all different solution types, indicating that, as may be expected, the number of nuclei is a smaller size of SPIONs and larger particle sizes in 28 J/cm² fluences increasing concentration SPIONs at 0.75, 0.21, 0.33, and 0.25, SPION ratio 53.89%, 29.28%, 30.99%, and 29.98% in Fig. 8b in various liquid types. This is also qualitatively supported by the overall decreasing coloration of the suspensions (insets in Fig. 7b). Instead, monotonically decrease spectra are observed in our experiments, except for a shoulder in the 200–300 nm range, as in research [23, 34, 53].

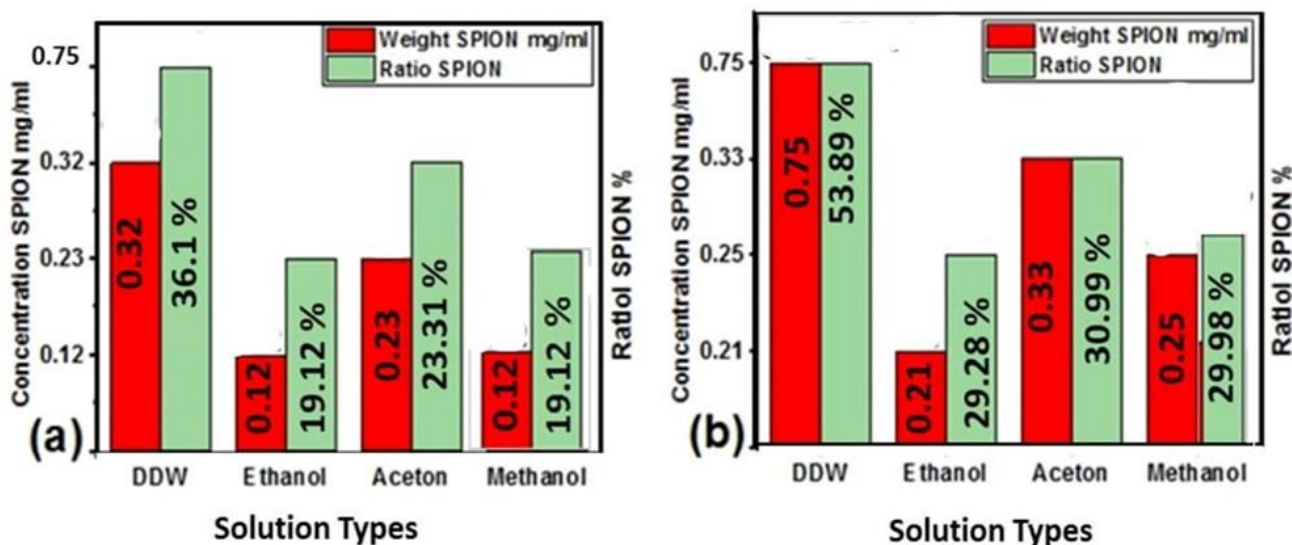


Figure 8: The relationship between SPIONs concentration (red bar), ratio (green bar), and laser fluence/ pulse at a- 10 J/cm² and b- 28 J/cm² after ablation Fe in different liquid types with wavelength 266 nm.

3.4 FTIR Results

After the strike process, the beaker containing the iron plate is moved periodically to obtain a homogeneous SPION colloid. Fig. 9 a,b,c and d shows the SPION NP produced in the different liquid types, DDW, ethanol, methanol, and acetone, respectively, with wavelength 266 nm and laser fluence of 28 J/cm² [54].

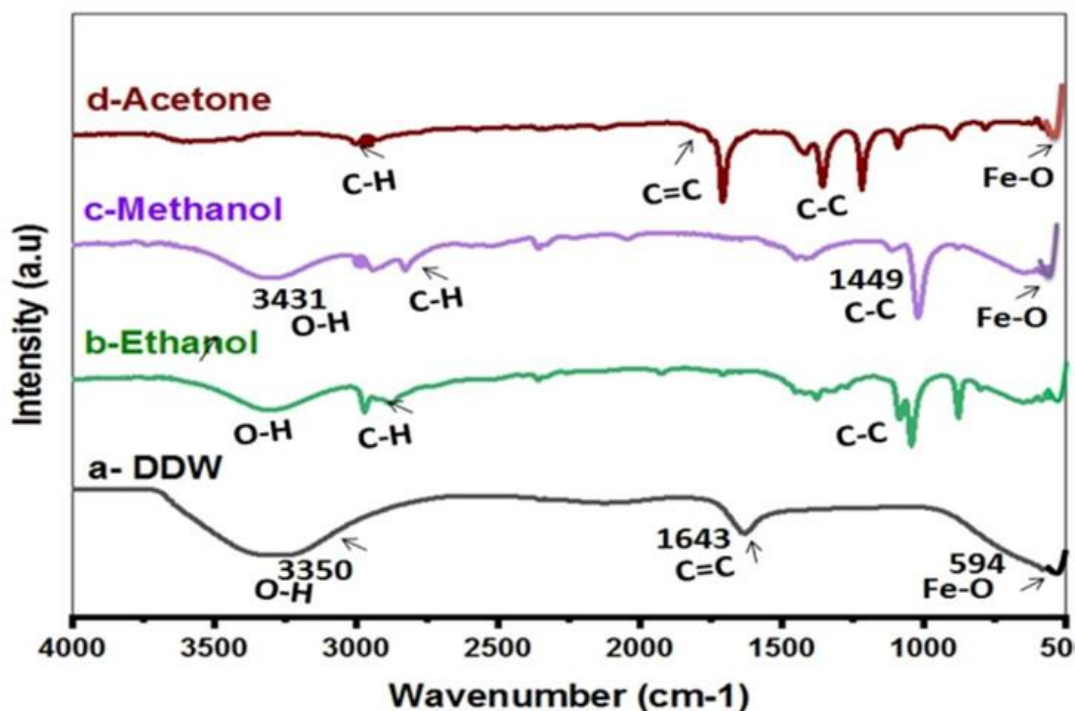


Figure 9: FTIR spectra of Fe_3O_4 NPs in a- DDW, b- ethanol, c- methanol, and d- acetone prepared at a laser fluence of 10 J/cm^2 with wavelength 266 nm.

The spectra of all colloidal NPs showed broadband in the range of $3000\text{--}3500 \text{ cm}^{-1}$, which was due to the extended vibration mode of the O-H in the three samples a, b, and c. More information on the chemical composition of the nanoparticles was obtained by comparing the FTIR spectrum of water, pure ethanol, pure methanol, and acetone with that of pure nanoparticles [55]. The intense band at approximately $3350\text{--}3430 \text{ cm}^{-1}$ is attributed to the water O-H stretching. The bending vibration modes in the ethanol spectra showed the additional peaks of C-H. This could be due to the formation of impurities such as OH [56] or the presence of organic compounds produced during the reaction of the laser beam and ethanol, or it could be coming from ethanol itself. These peaks (O-H stretching) were missing in the pure acetone spectrum (shown three peaks (594 , 1543 and 1633) cm^{-1} for Fe-O, C-C, and C=C, respectively). The absorption peak at 3431 cm^{-1} corresponds to the stretching vibration of OH indicating the presence of a large number of hydroxyl groups on the surface of the iron oxide nanoparticles, which increases the tendency to agglomeration in the synthesized SPIONs. Peaks at 1449 cm^{-1} in b, 1643 cm^{-1} in c, an additional peak at 2895 cm^{-1} in this sample are attributed to aliphatic H-C, and 1643 cm^{-1} in d is assigned to the SPION C=C stretching. The band appeared on the right shoulder of the spectrum at $\sim (500\text{--}700) \text{ cm}^{-1}$ in a, and the signal peak of $\sim 594 \text{ cm}^{-1}$ in all samples could be attributed to the Fe-O vibration bond [50, 57]. The respective metal oxides agree well with the results of other workers. All samples were observed to have the characteristic band $\sim 594 \text{ cm}^{-1}$, confirming the successful preparation of iron oxide NP using a simple top-bottom PLAIL approach. This is most likely due to the increase in the concentration of FeO NPs as acetone and ethanol. Thus, the FTIR results could indicate that the different types of liquids successfully served as stabilizing and capping agents during the Fe_3O_4 NPs synthesis process [58].

4. Conclusions

Briefly, we succeeded in preparing SPIONs by nanosecond laser operating with THG mode. The resultant composition of the Fe_xO_y NPS depends on the high-flux laser and the type of liquid. In all solutions except ethanol and methanol, nucleation was difficultly obtained at low laser fluence, resulting in a small number of nuclei and larger particle sizes, while at high energy densities, nucleation occurred simultaneously, resulting in a large number of nuclei and smaller particle sizes, especially in DDW and acetone obtained in a high concentration and SPIONs ratio at 0.75 and 0.25, and 53.89% and 29.89%, respectively at laser fluency 28 J/cm^2 . It showed in this work, that Fe_3O_4 nanoparticles size $<50 \text{ nm}$ and of quasi-cubical shape had stronger saturation magnetization and higher

magnetic performance. Finally, all types of liquids containing acetone, ethanol, and methanol led to the enhanced and increased concentrations formation of NPs with SPION phases, which are not detected in NPs generated in DDW. The produced Fe₃O₄ NPs from this research have been shown to have a high concentration and high stability for more samples without exaggeration in alcohol liquid such as acetone, methanol, and ethanol than in DDW. Therefore, these liquids are very suitable for biomedical applications, especially in drug delivery.

Acknowledgement

The authors acknowledge gratefully the technical support provided by the Laser Science and Technology Branch, Applied Sciences Department, University of Technology -Iraq.

Conflict of Interest

The authors declare that they have no conflict of interest.

References

- [1] D. Nath and P. Banerjee, "Author's personal copy Green nanotechnology – A new hope for medical biology," *Environ. Toxicol. Pharmacol.*, vol. 36, no. 3, pp. 997–1014, 2013.
- [2] K. B. Sutradhar and M. L. Amin, "Nanotechnology in Cancer Drug Delivery and Selective Targeting," *ISRN Nanotechnol.*, vol. 2014, pp. 1–12, 2014.
- [3] H. Chhipa, "Applications of nanotechnology in agriculture," *Methods Microbiol.*, vol. 46, pp. 115–142, 2019.
- [4] EJ Al Dine, Z Ferjaoui, J Ghanbaja, T Roques-Carmes, A. Hamieh T, J Toufaily, R Schneider, S Marchal, E Gaffet, H Alem. "Thermo-responsive magnetic Fe₃O₄@ P (MEO2MAX-OEGMA100-X) NPs and their applications as drug delivery systems." *International Journal of Pharmaceutics*. 2017 Nov 5;532(2):738-47.
- [5] BA Taha, N Ali, NM Sapiee, MM Fadhel, Mat RM Yeh, NN Bachok, Y Al Mashhadany, N Arsad. "Comprehensive review tapered optical fiber configurations for sensing application: trend and challenges. Biosensors". 2021 Jul 27;11(8):253.
- [6] T Iwamoto, T Ishigaki. "Fabrication of iron oxide nanoparticles using laser ablation in liquids". In *Journal of Physics: Conference Series* 2013 Jun 13 (Vol. 441, No. 1, p. 012034). IOP Publishing.
- [7] M. M. Elgaud *et al.*, "Pulse compressed time domain multiplexed fiber bragg grating sensor: a comparative study," *IEEE Access*, vol. 6, pp. 64427–64434, 2018.
- [8] A. J. Haider, M. A. Al-Kinani, and S. Al-Musawi, "Preparation and characterization of gold coated super paramagnetic iron nanoparticle using pulsed laser ablation in liquid method," in *Key Engineering Materials*, vol. 886, Trans Tech Publications Ltd, 2021, pp. 77–85.
- [9] B. A. Taha and L. Min, "Morphological Features and Divergence of SARS- CoV 2 and SARS-CoV Virus Using TEM Images," pp. 1–21, 2022.
- [10] H Naser, MA Alghoul, MK Hossain, N Asim, MF Abdullah, MS Ali, FG Alzubi, N Amin. "The role of laser ablation technique parameters in synthesis of nanoparticles from different target types". *Journal of Nanoparticle Research*. 2019 Nov;21(11):1-28.
- [11] B. Ahmed *et al.*, "Photonics enabled intelligence system to identify SARS - CoV 2 mutations," *Appl. Microbiol. Biotechnol.*, 2022.
- [12] B. A. Taha, "Perspectives of Photonics Technology to Diagnosis COVID–19 Viruses: A Short Review," *J. Appl. Sci. Nanotechnol.*, vol. 1, no. 1, pp. 1–6, 2021.
- [13] A. J. Haider, A. A. Jabbar, and G. A. Ali, "A review of Pure and Doped ZnO Nanostructure Production and its Optical Properties Using Pulsed Laser Deposition Technique," *J. Phys. Conf. Ser.*, vol. 1795, no. 1, 2021.
- [14] M. Al-Kinani, A. Haider, and S. Al-Musawi, "Study the Effect of Laser Wavelength on Polymeric Metallic Nanocarrier Synthesis for Curcumin Delivery in Prostate Cancer Therapy: In Vitro Study," *J. Appl. Sci. Nanotechnol.*, vol. 1, no. 1, pp. 43–50, Apr. 2021.
- [15] S. Al-Musawi *et al.*, "Smart nanoformulation based on polymeric magnetic nanoparticles and vincristine drug: A novel therapy for apoptotic gene expression in tumors," *Life*, vol. 11, no. 1, pp. 1–12, Jan. 2021.

- [16] A. J. Haider, R. A. Al-Rsool, A. A. Al-Tabbakh, A. N. M. Al-Gebori, and A. Mohamed, "Structural, morphological and optical properties of $\text{LiCo}_{0.5}\text{Ni}_{0.45}\text{Ag}_{0.05}\text{O}_2$ thin films," *AIP Conf. Proc.*, vol. 1968, pp. 0–8, 2018.
- [17] A. J. Haider, A. A. Al-Tabbakh, A. B. Al-Zubaidi, and R. A. Rsool, "Preparation and characterization of $\text{LiCo}_{0.5}\text{Ni}_{0.45}\text{Ag}_{0.05}\text{O}_2$ cathode material for lithium-ion battery," *J. Mater. Sci. Mater. Electron.*, vol. 29, no. 15, pp. 13277–13285, 2018.
- [18] N. Arsad, M. Li, G. Stewart, and W. Johnstone, "Intra-cavity spectroscopy using amplified spontaneous emission in fiber lasers," *J. Light. Technol.*, vol. 29, no. 5, pp. 782–788, 2011.
- [19] M. Muhanad Fadhel, H. Rashid, A. Essa Hamzah, M. S. Dzulkefly Zan, N. Abd Aziz, and N. Arsad, "Flat frequency comb generation employing cascaded single-drive Mach-Zehnder modulators with a simple analogue driving signal," *J. Mod. Opt.*, vol. 68, no. 10, pp. 536–541, 2021.
- [20] A. J. Haider, M. J. Haider, M. D. Majed, A. H. Mohammed, and H. L. Mansour, "Effect of Laser Fluence on a Microarray Droplets Micro-Organisms Cells by LIFT Technique," *Energy Procedia*, vol. 119, pp. 256–263, 2017.
- [21] A. J. Haider, K. A. Sukkar, A. H. Abdalsalam, A. F. Ali, S. H. Jaber, and T. T. A. Ridha, "Enhancement of the air quality and heat transfer rate of an air-conditioning system using a hybrid polypropylene nanofilter," *Process Saf. Environ. Prot.*, vol. 149, pp. 56–66, 2021.
- [22] A. J. Haider, A. Jasim Mohammed, S. S. Shaker, K. Z. Yahya, and M. J. Haider, "Sensing Characteristics of Nanostructured SnO_2 Thin Films as Glucose Sensor," *Energy Procedia*, vol. 119, pp. 473–481, 2017.
- [23] R. A. R. Abaas, A. J. Haider, F. A. Jabbar, and M. M. Hathal, "Characterisation of Fe Doped Layered Cathode Material as Nano-Rechargeable Batteries," *IOP Conf. Ser. Mater. Sci. Eng.*, vol. 987, no. 1, 2020.
- [24] C. Janzen and P. Roth, "Formation and characteristics of Fe_2O_3 nano-particles in doped low pressure $\text{H}_2/\text{O}_2/\text{Ar}$ flames," *Combust. Flame*, vol. 125, no. 3, pp. 1150–1161, 2001.
- [25] S. Shen, F. Kong, X. Guo, L. Wu, H. Shen, and M. Xie, "CMCTS stabilized Fe_3O_4 particles with extremely low toxicity as highly efficient near-infrared photothermal agents for in vivo tumor ablation". *Nanoscale*. 2013;5(17):8056-66.
- [26] M. J. Haider, A. A. Hadi, J. A. Saimon, and A. J. Haider, "Retraction Note: Investigation and improvement of layered lithium-ion nano-batteries by iron effect on storage energy efficiency (Journal of Nanoparticle Research, (2020), 22, 7, (205), 10.1007/s11051-020-04927-2)," *J. Nanoparticle Res.*, vol. 23, no. 8, p. 100081, 2021..
- [27] S. Shen *et al.*, "CMCTS stabilized Fe_3O_4 particles with extremely low toxicity as highly efficient near-infrared photothermal agents for in vivo tumor ablation," *Nanoscale*, vol. 5, no. 17, pp. 8056–8066, 2013.
- [28] M. A. Al-Kinani, A. J. Haider, and S. Al-Musawi, "Design and Synthesis of Nanoencapsulation with a New Formulation of $\text{Fe}@Au\text{-CS-CU-FA}$ NPs by Pulsed Laser Ablation in Liquid (PLAL) Method in Breast Cancer Therapy: In Vitro and In Vivo," *Plasmonics*, vol. 16, no. 4, pp. 1107–1117, Aug. 2021.
- [29] A. J. Haider, R. A. AL-Rsool, and M. J. Haider, "Morphological and Structural Properties of Cathode Compound Material for Lithium-Ion Battery," *Plasmonics*, vol. 13, no. 5, pp. 1649–1657, 2018.
- [30] M. Muniz-miranda, F. Muniz-miranda, and E. Giorgetti, "Spectroscopic and Microscopic Analyses of $\text{Fe}_3\text{O}_4 / \text{Au}$ Nanoparticles Obtained by Laser Ablation in Water,". *Nanomaterials*. 2020 Jan 10;10(1):132.
- [31] A. J. Haider, "Formulation of Curcumin in Folate Functionalized Polymeric Coated $\text{Fe}_3\text{O}_4 @ \text{Au}$ Core-Shell Nanosystem for Targeting Breast Cancer Therapy," pp. 1–18, 2022.
- [32] A. Haider and Z. N. Jameel, "Synthesis and Characterization of TiO_2 Nanoparticles via Sol- Gel Method by Pulse Laser Ablation Synthesis and Characterization of TiO_2 Nanoparticles",. *Eng. & Tech. Journal*. 2015 Nov;33(5):761-71.
- [33] S. H. Salim, R. H. Al-Anbari, and A. Haider, "Polysulfone/ TiO_2 Thin Film Nanocomposite for Commercial Ultrafiltration Membranes," *J. Appl. Sci. Nanotechnol.*, vol. 2, no. 1, pp. 80–89, Jan. 2022.

- [34] V. Amendola *et al.*, “Room-Temperature Laser Synthesis in Liquid of Oxide, Metal-Oxide Core-Shells, and Doped Oxide Nanoparticles,” *Chem. - A Eur. J.*, vol. 26, no. 42, pp. 9206–9242, 2020.
- [35] J. Lian, X. Duan, J. Ma, P. Peng, T. Kim, and W. Zheng, Hematite (α -Fe₂O₃) with Various Morphologies: Ionic Liquid-Assisted Synthesis. Formation Mechanism, and Properties. Vol. 3, NO. (2009)11 PP. 3749–3761
- [36] S. Al-Musawi, M. Jawad, N. Khazal, and K. Hindi, “Folated-nanocarrier for paclitaxel drug delivery in leukemia cancer therapy Medical Microbiology View project cancer therapy View project,” 2018. *Journal of Pharmaceutical Sciences and Research*. 2018 Apr 1;10(4):749-54.
- [37] M. A. Al-Kinani, A. J. Haider, and S. Al-Musawi, “High Uniformity Distribution of Fe@Au Preparation by a Micro-Emulsion Method,” in *IOP Conference Series: Materials Science and Engineering*, Nov. 2020, vol. 987, no. 1.
- [38] A. Tsubaki, C. A. Zuhlke, R. Bell, T. P. Anderson, and D. R. Alexander, “Micro/nanostructures formation by femtosecond laser surface processing on amorphous and polycrystalline Ni₆₀Nb₄₀,” *Appl. Surf. Sci.*, vol. 396, pp. 1170–1176, Feb. 2017.
- [39] J. M. J. Santillán *et al.*, “Optical and Magnetic Properties of Fe Nanoparticles Fabricated by Femtosecond Laser Ablation in Organic and Inorganic Solvents,” *ChemPhysChem*, vol. 18, no. 9, pp. 1192–1209, 2017.
- [40] R. Nadarajah *et al.*, “Article formation of fe-ni nanoparticle strands in macroscopic polymer composites: Experiment and simulation,” *Nanomaterials*, vol. 11, no. 8, 2021.
- [41] M. Fakhar-e-Alam, A. Mahmood, S. Nasir, M. Saadullah, M. Waseem Akram, and M. Willander, *Gadolinium-Doped Iron Nanostructures Decorated with Novel Drugs for Magnetic Resonance Imaging, Photodynamic, and Photothermal Therapy Applications*. 2020.
- [42] F. A. Fadhil, F. I. Sultan, A. J. Haider, and R. A. Rsool, “Preparation of poison gas sensor from WO₃ nanostructure by pulsed laser deposition,” in *AIP Conference Proceedings*, 2019, vol. 2190.
- [43] A Qona’ah, I Nurhasanah, A.Khumaeni, "Synthesis of Tin Oxide Nanoparticles by Pulsed Laser Ablation Method Using Low-Energy Nd: YAG Laser as an Antibacterial Agent". *InJournal of Nano Research* 2021 (Vol. 68, pp. 114-122). Trans Tech Publications Ltd.
- [44] V. Amendola *et al.*, “Magnetic iron oxide nanoparticles with tunable size and free surface obtained via a ‘green’ approach based on laser irradiation in water,” *Journal of Materials Chemistry*, vol. 21, no. 46. pp. 18665–18673, 2011.
- [45] C. Barelle, V. Chabroux, and D. Favier, “Modeling of the time trial cyclist projected frontal area incorporating anthropometric, postural and helmet characteristics,” *Sport. Eng.*, vol. 12, no. 4, pp. 199–206, 2010.
- [46] S. Dadashi, R. Poursalehi, and H. Delavari, “Structural and Optical Properties of Pure Iron and Iron Oxide Nanoparticles Prepared via Pulsed Nd:YAG Laser Ablation in Liquid,” *Procedia Mater. Sci.*, vol. 11, pp. 722–726, 2015.
- [47] G. Alva, L. Liu, X. Huang, and G. Fang, “Thermal energy storage materials and systems for solar energy applications,” *Renew. Sustain. Energy Rev.*, vol. 68, no. October 2016, pp. 693–706, 2017.
- [48] G. Alva, Y. Lin, and G. Fang, “An overview of thermal energy storage systems,” *Energy*, vol. 144, pp. 341–378, 2018.
- [49] F. Al-Obaidy and F. A. Mohammadi, “Predictions optimal routing algorithm based on artificial intelligence technique for 3D NoC systems,” *Microsyst. Technol.*, vol. 27, no. 9, pp. 3313–3323, 2021.
- [50] I. Hasan, K. Khashan, and A. Hadi, “Study of the Effect of Laser Energy on the Structural and Optical Properties of TiO₂ NPs Prepared by PLAL Technique,” *J. Appl. Sci. Nanotechnol.*, vol. 2, no. 1, pp. 11–19, 2022.
- [51] H. Li, L. Qin, Y. Feng, L. Hu, and C. Zhou, “Preparation and characterization of highly water-soluble magnetic Fe₃O₄ nanoparticles via surface double-layered self-assembly method of sodium alpha-olefin sulfonate,” *J. Magn. Magn. Mater.*, vol. 384, pp. 213–218, 2015.

- [52] P. Simamora, C. S. Saragih, D. P. Hasibuan, and J. Rajagukguk, "Synthesis of nanoparticles Fe₃O₄/PEG/PPy-based on natural iron sand," *Mater. Today Proc.*, vol. 5, no. 7, pp. 14970–14974, 2018.
- [53] M. J. Rivera-Chaverra, E. Restrepo-Parra, C. D. Acosta-Medina, A. Mello, and R. Ospina, "Synthesis of oxide iron nanoparticles using laser ablation for possible hyperthermia applications," *Nanomaterials*, vol. 10, no. 11, pp. 1–13, 2020.
- [54] A. Hussein, M. S. Abd-Elhady, M. N. El-Sheikh, and H. T. El-Metwally, "Improving Heat Transfer Through Paraffin Wax, by Using Fins and Metallic Strips," *Arab. J. Sci. Eng.*, vol. 43, no. 9, pp. 4433–4441, 2018.
- [55] A. J. Haider, R. H. Al-Anbari, G. R. Kadhim, and C. T. Salame, "Exploring potential Environmental applications of TiO₂ Nanoparticles," *Energy Procedia*, vol. 119, pp. 332–345, 2017.
- [56] M. Yusefi *et al.*, "Green synthesis of Fe₃O₄ nanoparticles stabilized by a garcinia mangostana fruit peel extract for hyperthermia and anticancer activities," *International Journal of Nanomedicine*, vol. 16, pp. 2515–2532, 2021.
- [57] M. Alheshibri, S. Akhtar, A. Al Baroot, K. A. Elsayed, H. S. Al Qahtani, and Q. A. Drmosh, "Template-free single-step preparation of hollow CoO nanospheres using pulsed laser ablation in liquid enviromen," *Arab. J. Chem.*, vol. 14, no. 9, p. 103317, 2021.
- [58] T. Ahn, J. H. Kim, H. M. Yang, J. W. Lee, and J. D. Kim, "Formation pathways of magnetite nanoparticles by coprecipitation method," *J. Phys. Chem. C*, vol. 116, no. 10, pp. 6069–6076, 2012.
- [59] Y. P. Yew *et al.*, "Green biosynthesis of superparamagnetic magnetite Fe₃O₄ nanoparticles and biomedical applications in targeted anticancer drug delivery system: A review," *Arab. J. Chem.*, vol. 13, no. 1, pp. 2287–2308, 2020.